RSC Advances

PAPER

View Article Online
View Journal | View Issue



Cite this: *RSC Adv.*, 2025, **15**, 15375

# Enhancement of biogas production using nanostructured magnetite ($Fe_3O_4$) in a biodigester fed with Peruvian guinea pig manure†

Rosa Flores Vargas, William Eduardo Gómez Hernández, Karenina Ela Macazana López, Clemente Alfredo Luyo Caycho, Yelstin Adrian Muñoz Baca, Harry Anderson Rivera Tito and María Esther Quintana Cáceda *

Magnetite nanoparticles were used to increase biogas production in a biodigester fed with Peruvian guinea pig (*Cavia porcellus*) manure (PGPM). The nanoparticles were synthesized *via* two different methods—coprecipitation and polyol—and thus showed different sizes of 410.7 nm and 34.03 nm, respectively. Likewise, various configurations were tested using three distinct $Fe_3O_4$ proportions, with each configuration tested in triplicate biodigesters. The coprecipitation trial with $Fe_3O_4$ was tested with an initial substrate of 5.57 g of chemical oxygen demand (COD) and 0.96 g of volatile solids (VSs) as inoculum. This ferrous additive led to a methane production increase of up to 9.61%, with a biodegradability of 57.91%. At the same time, the polyol trial with $Fe_3O_4$ was tested with an initial substrate of 34.47 g of COD and 0.80 g VS as inoculum, increasing methane production by up to 64.5% with a biodegradability of up to 8.56%. Moreover, the inhibitory effect of the synthesized $Fe_3O_4$, which was inconsequential for bacterial growth, was analyzed. Therefore, these nanoparticles have been shown to support methanogenic bacteria in enhancing methane production.

Received 6th January 2025
Accepted 11th March 2025

DOI: 10.1039/d5ra00102a

rsc.li/rsc-advances



## Introduction

Biogas is a gaseous mixture primarily composed of methane ($CH_4$) and carbon dioxide ($CO_2$); it also contains traces of other gases such as hydrogen ($H_2$) and hydrogen sulfide ($H_2S$) and is formed through the decomposition of natural organic matter (OM) in an anaerobic environment.[1,2] Among these gases, $CH_4$ stands out for its calorific value of around 7.0 kWh $m^{-3}$ (considering an average 65% $CH_4$ and 35% $CO_2$ biogas composition).[3] Furthermore, among the trace gases, $H_2S$ is noteworthy as it is responsible for the strong and unpleasant odor associated with biogas.[4]

As its name suggests, biogas is naturally formed through a biological pathway and is therefore widely present in nature.[1] It can be found in swamps, ruminants' stomachs,[5] and sanitary landfills.[6] In the latter, when there are high OM levels, such as in landfill leachate, its decomposition produces biogas due to the low solubility of oxygen ($O_2$) in water. This gas is chemically similar to the natural gas found in fossil fuel deposits.[4] In terms of energy content, 1 $m^3$ of biogas is equivalent to 0.6–0.65 L of petroleum.[3]

Moreover, the European Union retrieves methane ($CH_4$) from sanitary landfills. For example, Germany leads in biogas production owing to its positive legal framework established in 2000 for renewable energy sources, which has promoted the development of biogas facilities throughout the country.[1] Currently, there are over 10 000 facilities across Germany.[7] Similarly, in Asia, thanks to programs that fomented the construction of digesters,[3] China has over 100 000 biogas plants.[7] This overview stands in stark contrast to Peru's efforts, as Peru is still far from reaching the renewable energy production goal set for 2030, which is 20%.[8] As of 2022, Peru has converted only 5.9% of its energy matrix to unconventional renewable energy,[9] of which only 0.1% is derived from biomass,[10] despite the country's potential for renewable energy production (solar, wind, and biomass).[11] Likewise, Peru generates a large volume of agricultural and commercial fishing waste, which is discarded,[12] although it could be used for biogas production and thus tackle three major national needs: (1) improve organic waste disposal sanitation; (2) generate renewable energy and (2) supply stabilized materials, such as biofertilizer, that can be used in agriculture.[3] Farm animal waste has already been used in biogas and energy production, with an array of different applications according to Monteros *et al.*[13]

Biogas production occurs through a complex biotechnological process of anaerobic digestion, where a consortium of bacteria degrades the OM in a coordinated manner.[4] The essential condition to ensure the success of the process is the

*Center for the Development of Advanced Materials and Nanotechnology, National University of Engineering, Av. Tupac Amaru 210, Lima 25, Peru. E-mail: mquintana@uni.edu*

† Electronic supplementary information (ESI) available. See DOI: https://doi.org/10.1039/d5ra00102a

absence of $O_2$. Biochemical and microbiological studies have thus far divided the process into four phases: hydrolysis, acidogenesis, acetogenesis, and methanogenesis.[3] Anaerobic digestion has been extensively studied. However, despite being a promising method for treating large quantities of waste, it remains a low-efficiency process, which limits its ability to compete in the current fuel market.[14] Since hydrolysis is the rate-limiting step of the process, several studies have focused on this phase to make the digestion process more efficient using chemical or physical pretreatments, such as the one reported by Hu *et al.*[14] where oxidative methods were applied to enhance the degradation rate of sludge from a water treatment plant. Other studies evaluated the effect of component addition during digestion, as reported by Casals *et al.*[15] who investigated the effect of adding magnetite ($Fe_3O_4$) nanoparticles of 7 nm into an anaerobic reactor for waste treatment.

Their results showed that biogas production per gram of OM increased by up to 180% when working with 100 ppm of $Fe_3O_4$, approximately 2.8 times the typical output. Huamán *et al.*[16] also evaluated the effect of adding $Fe_3O_4$ particles sized 0.5–1.0 mm during anaerobic digestion. They used pig manure and evaluated the effect of two $Fe_3O_4$ dosages: 8 g and 12 g. The best results were obtained with 8 g of $Fe_3O_4$, yielding $3.82 \times 10^{-2}$ N $m^3$ of $CH_4$ $kg^{-1}$ of volatile solids (VSs). It is important to note that each OM source possesses different biogas production potentials. Generally, manure from polygastric animals generates less biogas than that from monogastric animals.[17] According to the Food and Agriculture Organization (FAO),[3] carbon (C) and nitrogen (N) are the main nutrients for methanogenic bacteria, both of which are present in larger quantities in PGPM compared with horse, cow, bird or pig manure.[18]

Villargaray *et al.*[19,20] maintain that the average amount of guinea pig manure produced by females is 28.15 g per day and 31.03 g per day for males, which implies an average daily production of 801.19 tons of guinea pig excrement per day (considering the number of guinea pigs in 2021 reported by MIDAGRI: approximately 25820 000 guinea pigs).[21]

Therefore, this study focuses on the effect of $Fe_3O_4$ particles on biogas production using PGPM under standard conditions, taking into account the geography and the diet of the animals *in situ*. The effect of the nanostructured particles was evaluated using a laboratory-scale biogas prototype reactor consisting of 500 mL bottles with hermetically sealed caps adapted for this purpose. They were used to directly quantify the amount of $CH_4$ *via* volumetric displacement, produced through the synergy between the OM, microorganisms, and $Fe_3O_4$ nanoparticles. Finally, this study aims to contribute to the enhancement of biogas production in sectors dedicated to the use of guinea pig manure.

## Materials and methods

### Chemical reagents

The materials used for the synthesis and methanogenic activity tests are listed below: Iron nitrate (III) nonahydrate ($Fe(NO_3)_3 \cdot 9H_2O$, ≥98%), Sigma-Aldrich. Triethylene glycol ($HO(CH_2CH_2O)_3H$, ≥98%), Merck. Ethyl acetate ($CH_3COOC_2H_5$, ≥98), Merck. Ethanol ($C_2H_6O$, 99.5%), Spectrum Chemical. Iron chloride (II) ($FeCl_2$, 99%), J. T. Baker. Iron chloride (III) ($FeCl_3$, 97%), Central Drug House (CDH). Hydrochloric acid (HCl, 37%), Spectrum Chemical. Ammonium hydroxide ($NH_4OH$, 30%), Merck. Sodium hydroxide (NaOH, ≥97%), Merck. Bromothymol blue ($C_{27}H_{28}Br_2O_5S$), Merck.

### Inoculum

The bacterial consortium (Fig. 1a) was collected from a biodigester of Universidad Nacional Agraria La Molina (UNALM). Moreover, the analyses of total solids (TS) and volatile suspended solids (VSS) were carried out at the SLab Peru testing and research laboratory (Table 1). The VSS/TS ratio was 0.38. This means that the amount of bacterial biomass in the inoculum was approximately 38% by mass.

### Raw material

Dried guinea pig manure collected (Fig. 1b) from the UNALM cages was used as a feedstock bio-substrate providing MO to each experiment. Its physicochemical characteristics, such as TS, were analysed at the SLab Peru testing and research laboratory. At the same time, the percentages of carbon (C%), nitrogen (N%), carbon-to-nitrogen ratio (C/N), and moisture (H%) were determined at the Soil Laboratory of the Faculty of Agricultural Engineering of the UNALM (Table 2).

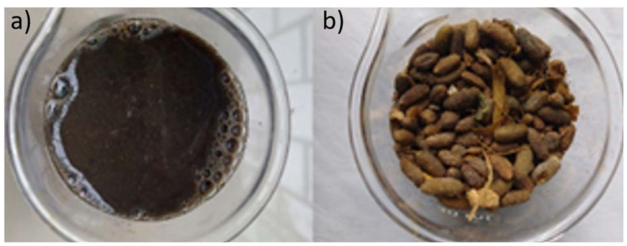


Fig. 1 (a) Bacterial inoculum and (b) dry *Cavia porcellus* manure.

Table 1 Values of variables analysed in the inoculum

| Analysis | Results |
|---|---|
| TS | 48 200 mg $L^{-1}$ |
| VSS | 18 200 mg $L^{-1}$ |

Table 2 Analysed parameters of guinea pig manure

| Analysis | Results (%) |
|---|---|
| TS | 79.42 |
| C | 44.95 |
| N | 2.04 |
| C/N | 22.03 |
| H | 25.04 |

### Microbial growth support

The salts necessary for bacterial growth were prepared following the guidelines of Chernicharo *et al.*[22,23] and the amounts reported by Cendales *et al.*[24] using a Balch-type and reducing solution.

### Magnetite ($Fe_3O_4$) synthesis

**Coprecipitation method.** This is the simplest and most efficient chemical route to produce magnetic particles.[25–28] $Fe_3O_4$ was prepared using a stoichiometric mixture of ferric and ferrous salts (eqn (1)). Thermodynamically, $Fe_3O_4$ precipitation is expected when a stoichiometric ratio of 2 : 1 ($Fe^{3+}/Fe^{2+}$) is maintained in an alkaline medium (pH between 8 and 14) and an inert environment since $Fe_3O_4$ is unstable and sensitive to oxidation, which would lead to the formation of maghemite ($\gamma$-$Fe_2O_3$). However, oxygen is not the only oxidizing agent for $Fe_3O_4$, as shown in eqn (2); oxidation can also occur *via* electron or ion transfer, depending on the pH of the suspension.[29]

$$Fe^{2+} + 2Fe^{3+} + 8OH^- \rightarrow Fe_3O_4 + 4H_2O \quad (1)$$

$$Fe_3O_4 + 2H^+ \rightarrow \gamma\text{-}Fe_2O_3 + Fe^{2+} + H_2O \quad (2)$$

The main advantage of this method is that a large number of particles can be synthesized albeit at the cost of a limited size distribution. In this study, $Fe_3O_4$ was synthesized following the method described by Puca *et al.*,[29] with slight modifications. The experimental setup is shown in Fig. 2a. $FeCl_3$ and $FeCl_2$ were used as precursor salts, and 50 mL solutions were prepared, with each salt dissolved in HCl. Both solutions were poured into a three-necked flask equipped with a magnetic stirring bar. The reaction was conducted in an inert environment, with $N_{2(g)}$ bubbled into the system for over 5 min. The flask was then heated to about 80 °C, and synthesis started by dropwise adding 50 mL of $NH_4OH$ (1 : 4). Thereafter, $Fe_3O_4$ was washed with distilled water until the supernatant reached a pH of ≈7. Finally, the precipitate was poured into a Petri dish and stored in a desiccator for further use.

**Polyol method.** This is a chemical reduction method to synthesize nanoparticles by reducing a portion of a salt.[30] The method involves suspending the precursor (iron salt $Fe(NO_3)_3 \cdot 9H_2O$) in a liquid polyol (*e.g.* triethylene glycol (TEG)).[31,32] Vega *et al.*[33] has described in detail the reaction pathways involved in each step of nanoparticle formation. The resulting suspension is heated to approximately the boiling point of the polyol, during which a solvolysis process occurs in the initial stage (eqn (3)).

In parallel, the precursor metal dissolves in the diol, thereby reducing the salt into iron complexes, which subsequently decompose and produce intermediate species (denoted as FeAx) (eqn (4)). These species act as nanoparticle cores in the subsequent step (eqn (5)) and serve as building blocks for their self-assembly and growth.

$$Fe(NO_3)_3 + TEG \leftrightarrow Fe(NO_3)_2TEG + NO_3^- \quad (3)$$

$$Fe(NO_3)_2TEG \rightarrow FeAx \quad (4)$$

$$FeAx \leftrightarrow Fe_3O_4 \quad (5)$$

In this regard, $Fe_3O_4$ nanoparticles were prepared using the precursor salt $Fe(NO_3)_3 \cdot 9H_2O$ and TEG as the surfactant-reducing agent. First, the system shown in Fig. 2b was brought to optimum conditions. Second, the precursor salt, TEG, and a magnetic stir bar were added to the three-necked flask. The reaction was carried out at three different temperatures under an inert $N_{2(g)}$ atmosphere: (1) 30 minutes at 120 °C, (2) 30 minutes at 180 °C, and (3) 60 minutes at 280 °C. Once the reaction was complete, the resulting product was poured into a beaker, and flocculation of $Fe_3O_4$ was carried out using ethyl acetate and ethanol. The process was repeated until the entire product had flocculated and the supernatant became colorless.

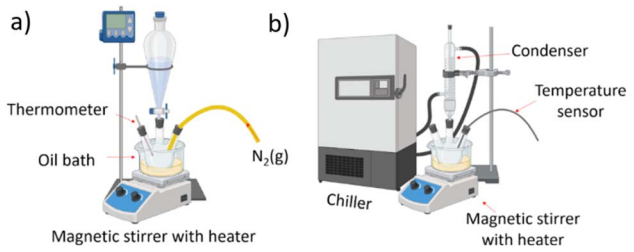


Fig. 2 Schematic representation of the apparatus for $Fe_3O_4$ synthesis using the coprecipitation (a) and polyol (b) methods.

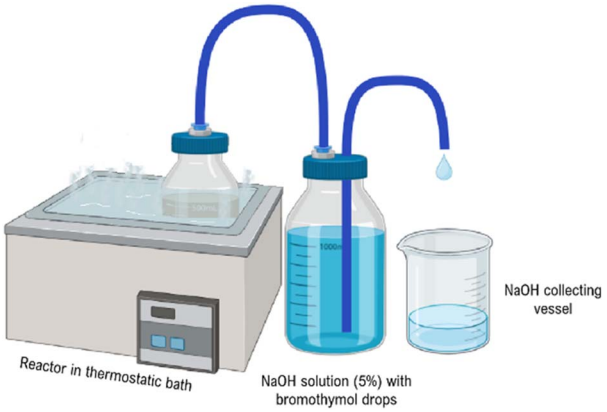


Fig. 3 Schematic representation of the MAT system mounted.

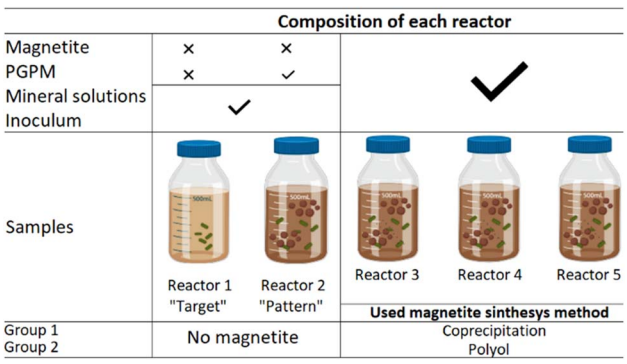


Fig. 4 Schematic of the whole system assembly for nanoparticle evaluation and biogas production.

Finally, the precipitate obtained was dispersed in ethanol and stored in a desiccator.

### Specific methanogenic activity (SMA)

There are different methods for testing SMA. The one used as a basis for this work is described in the book Anaerobic Reactors[23] and recommendations from the experiments developed by Córdova *et al.*[34] and Cendales *et al.*[24] To perform the tests, two glass bottles of 500 mL and 1000 mL were used. These were joined using a snap connector in the cap, through which a small hose allowed the biogas to flow from one container to the other. The digestion process was carried out inside the 500 mL bottle. In addition, 53 mL of inoculum, 32 mL of dissolved manure and 395 mL of mineral salt solution were added to each reactor.

To measure gas production during the digestion process, the volumetric displacement method was used (Fig. 3). Each 1 L bottle was prepared with a 5% NaOH solution and a few drops of bromothymol blue. Additionally, the bottle cap contained a hose extended to the bottom of the bottle so that the displaced soda could flow due to the pressure of the generated biogas, while the other end of the hose rested on a glass collector. The tests were repeated three times under mesophilic conditions (35 °C). A total of five reactors were evaluated per run (the composition of each one is shown in Fig. 4). The first reactor was the target, the second was the pattern, and the rest were evaluated to assess the effect of different $F_3O_4$ quantities. Group 1 evaluated the performance of cop-$Fe_3O_4$ (magnetite synthesized *via* the coprecipitation method) with an initial organic loading of 5.57 g COD. Group 2 used pol-$Fe_3O_4$ (magnetite synthesized *via* the polyol method) and had an organic loading of 34.47 g COD, where higher performance was achieved when working up to 100 ppm[16] (100 mg per litre of mixture).

### Characterization equipment

**Light dynamic dispersion (LDS).** The 90 Plus Particle Size Analyser from Brookhaven Instruments was used. It operated using a refraction index ($n$) of 2.36 for $Fe_3O_4$. The LDS samples were prepared by dispersing a small amount of $Fe_3O_4$ powder in TEG. The suspension was sonicated with an amplitude of 40% per minute. Thereafter, the sample was poured on disposable cuvettes with 4 optical windows from BRAND.

**X-ray diffraction.** The D8 ADVANCE model from Bruker brand diffractometer was used to assess the crystal properties of $Fe_3O_4$. This was operated under a current of 30 mA, 40 kV, ($2\theta$) range of 10°–90° and 2.5° per min and a wavelength of 1.5418 Å ($\lambda_{Cu\alpha}$).

**Scanning electron microscopy.** Model EVO-MA10 of brand ZEISS instruments was used to explore the $Fe_3O_4$ morphology. This was operated under 20 kV and an 8.5 mm working distance between the objective lens and the sample camera.

## Results and discussion

The quantities of $Fe_3O_4$ obtained from the synthesis routes are reported in Table 3. These measurements represent averages and do not account for the weight of small particles lost during the washing process.

Table 3 Quantities of powder $Fe_3O_4$ obtained through synthesis

| Method | Quantity |
|---|---|
| Coprecipitation | 1.34 g |
| Polyol | 0.48 g |

Therefore, the average crystallite size was calculated from the analysis of the most intense diffraction peaks using the Debye–Scherrer equation (eqn (6)):

$$D = \frac{k \times \lambda}{\beta \cos \theta}, \quad (6)$$

where $D$ represents the crystallite grain size (Å), $k$ is a constant with a value of 0.9, $\lambda$ is the incident radiation wavelength (Å) (in this case the incident radiation was CuK$\alpha$, $\lambda = 1.54$ Å), $\beta$ is the width of the peak at half its strongest intensity (rad) and $\theta$ represents the diffraction angle.[35] The cop-$Fe_3O_4$ showed characteristic $Fe_3O_4$ signals at $2\theta$ angles with intensities at 30.16°, 35.60°, 43.22°, 53.72°, 57.14° and 62.83° (Fig. 5) and an average

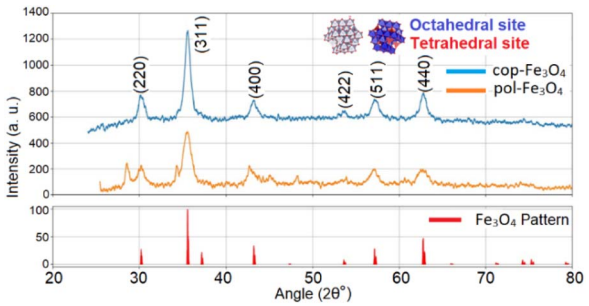


Fig. 5 $Fe_3O_4$ pattern, cop-$Fe_3O_4$ and pol-$Fe_3O_4$ X-ray diffractograms.

Table 4 Lattice parameter regarding each cop-$Fe_3O_4$ crystallographic plane

| Miller index | $2\theta$ (°) | $d$ | $a$ (Å) |
|---|---|---|---|
| (220) | 30.16 | 2.96 | 8.38 |
| (311) | 35.60 | 2.52 | 8.36 |
| (400) | 43.22 | 2.09 | 8.37 |
| (422) | 53.72 | 1.71 | 8.36 |
| (511) | 57.14 | 1.61 | 8.38 |
| (440) | 62.83 | 1.48 | 8.37 |
| Average | — | — | 8.37 |

Table 5 Lattice parameter regarding each pol-$Fe_3O_4$ crystallographic plane

| Miller index | $2\theta$ (°) | $d$ | $a$ (Å) |
|---|---|---|---|
| (220) | 30.24 | 2.96 | 8.36 |
| (311) | 35.57 | 2.52 | 8.37 |
| (400) | 42.71 | 2.12 | 8.47 |
| (422) | 53.92 | 1.70 | 8.33 |
| (511) | 57.18 | 1.61 | 8.37 |
| (440) | 62.49 | 1.49 | 8.41 |
| Average | — | — | 8.38 |

grain size of 8.92 nm (Table 4). Pol-$Fe_3O_4$, displayed similar intense peaks at 30.24°, 35.57°, 42.71°, 53.92°, 57.18° and 62.49° (Fig. 5), achieving medium crystallite sizes, as depicted in Table 5, corresponding to an average $Fe_3O_4$ crystal size of 6.78 nm. Both samples were compared with the maghemite diffraction pattern from the XRD software library, showing analogous intensities at 28.57°, 34.34° and 48.25°, suggesting that the prepared samples are isostructural ferromagnetic iron oxides and $Fe_3O_4$.[36,37]

*K* factor depends on the geometry, although a commonly used value is 0.89. This approximation is based on the assumption of perfectly spherical particles and is applicable to crystals with sizes up to 100 or 200 nm,[38] as peak broadening decreases with an increasing particle size. In this regard, Bragg's law allows the determination of the lattice parameters of a crystal structure. cop-$Fe_3O_4$ and pol-$Fe_3O_4$ results are shown in Tables S1 and S2,† respectively. In addition, the $Fe_3O_4$ structure is a characteristic FCC of the inverse spinel type, featuring 8 tetrahedral sites occupied by $Fe^{2+}$ and 16 octahedral sites equally occupied by $Fe^{2+}$ and $Fe^{3+}$.[39] As an FCC structure, it has only one lattice parameter, which can be calculated from each crystallographic plane using Eq. (7) and (8).

$$\lambda_{CuK\alpha} = 2 \times d \times \sin(\theta) \quad (7)$$

$$\frac{1}{d^2} = \frac{h^2 + k^2 + l^2}{a^2} \quad (8)$$

Moreover, it is well known in crystallography that *h*, *k*, and *l* are the Miller indices of a crystallographic plane. The calculated values for cop-$Fe_3O_4$ and pol-$Fe_3O_4$ are shown in Tables 4 and 5, respectively.

Both materials have a similar average lattice parameter of ≈8.39 Å, which was also reported by G. Peña *et al.*[40]

Measuring $CH_4$ production content in biogas through the volumetric displacement method demonstrated daily biogas production by applying nanoparticles (Fig. 6a and b). In Group 2, the $Fe_3O_4$ effect is highly remarkable. Using 48 mg of pol-$Fe_3O_4$ (100 ppm) with a smaller particle size (according to DLS,[41] Fig. S1 and eqn (S1)–(S3)†), $CH_4$ production increased by up to 64.5% compared with the sample without $Fe_3O_4$. Nonetheless, the use of larger cop-$Fe_3O_4$ (100 ppm) (0.4 μm particle size) resulted in only a 9.61% increase. Therefore, both tests confirm that the optimal amount of $Fe_3O_4$ is around 100 ppm. Although, particle size also affects biogas production, when particles are too large (800 nm to 4.5 μm), they become inefficient.[42] Thus, the increase in biogas is attributed to magnetite's role as a mediator between the donors and acceptors of chemical species involved in methanogenesis.[42–44] According to the results, this suggests that increased biogas production was due to the symbiotic association between bacteria and iron nanoparticles, according to Baek *et al.*[45] and Wang *et al.*,[46] whose studies focused on investigating the role of iron compounds such as $Fe_3O_4$ in the performance of anaerobic digestion. Biogas production modelling can follow a sigmoid function.[42,47] The most commonly used function is the modified Gompertz function (eqn (9)). Using this equation, the average daily gas production rate, the lag time, and the mass production estimate were obtained:

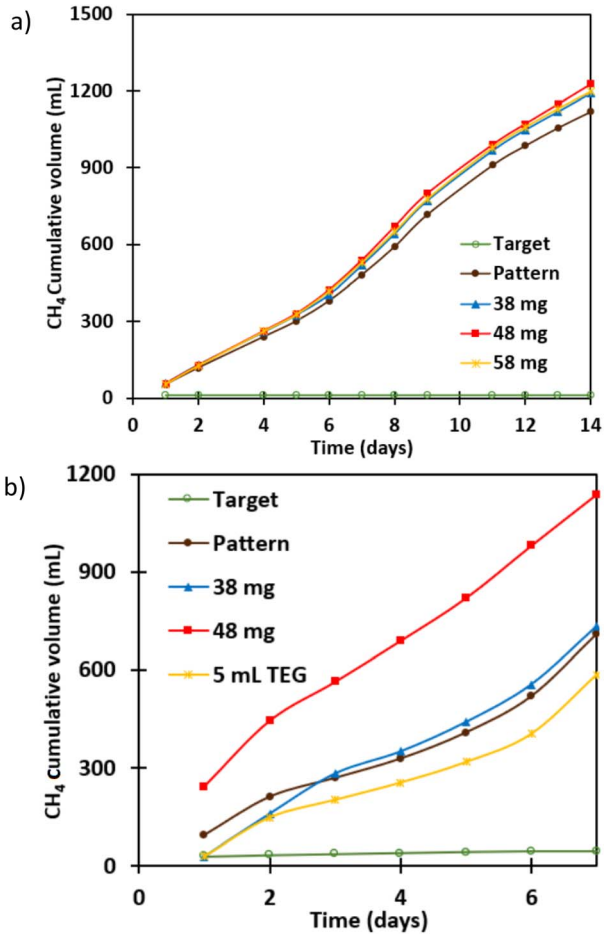


Fig. 6 Total $CH_4$ production using (a) cop-$Fe_3O_4$ (mg) and (b) pol-$Fe_3O_4$ (mg) groups.

$$M_m = a \times e^{-e\left(\frac{b \times e}{a}\right) \times (\lambda - t) + 1}, \quad (9)$$

where *a* corresponds to maximum $CH_4$ production (mL), *b* is the average production rate (mL per day) and $\lambda$ is the lag time.

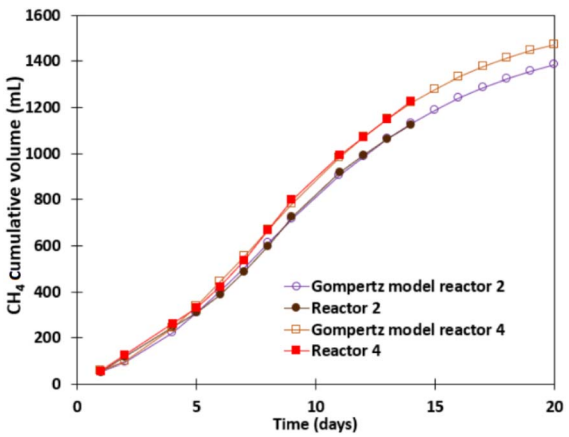


Fig. 7 Gompertz model to reactors 2 and 4 of enhanced $CH_4$ production with cop-$Fe_3O_4$.

Table 6 Biodegradability (Bd) percentage of each trial

| | Results | |
|---|---|---|
| Analysis | Bd target (%) | Bd 100 ppm (%) |
| Coprecipitation trial | 52.88% | 57.91% |
| Polyols trial | 5.30% | 8.56% |

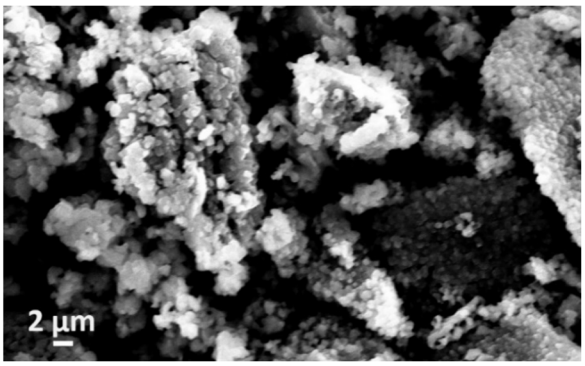


Fig. 8 SEM image of $Fe_3O_4$ used to evaluate biological inhibition.

Table 7 Biological study results

| | $10^8$ UFC $mL^{-1}$ | | | | |
|---|---|---|---|---|---|
| Analysis | 0 h | 24 h | 48 h | 96 h | 120 h |
| Inoculum (control) | 9.7 | 9.5 | 9.0 | 8.0 | 7.0 |
| Inoculum plus $Fe_3O_4$ | 9.7 | 9.3 | 8.9 | 8.1 | 6.9 |

Furthermore, Gompertz's correlation in $CH_4$ production (as shown in Fig. 7) from the corresponding reactors is shown in Fig. 6a. It is possible to determine the theoretical maximum $CH_4$ that could be produced from a specific organic load. Theoretically, 2.61 g of COD can be converted into 1 L of $CH_4$ under standard conditions if the organic matter is fully converted to methane.[22] In the case of the trials with pol-$Fe_3O_4$, an additional amount of PGPM corresponding to 34.47 g COD was used, whereas the trials with cop-$Fe_3O_4$ used a corresponding amount of 5.57 g COD. The results for these trials are shown in Table 6.

Additionally, Table 8 provides a summary of various sources regarding the $CH_4$ vol. Produced relative to volatile solids in the feed and the COD of the substrate.

The models are experimental extrapolation since most studies on biogas have test periods of 30 or 60 days. For this reason, the Gompertz mathematical model, commonly applied in such cases, was used for approximation (eqn (9) (S4) and (S5)†).

In the assays with pol-$Fe_3O_4$, an average increase of up to 64.5% in biogas production over 7 days was observed when 100 ppm of $Fe_3O_4$ nanoparticles were added, compared with a bioreactor without them. According to the Gompertz model, this increase would reach 45.81% after 40 days, indicating the point of maximum biogas production. In contrast, for the cop-$Fe_3O_4$ assays, an average increase of 9.61% was observed over 14 days with the addition of 100 ppm of $Fe_3O_4$ nanoparticles. Based on the Gompertz model, this increase would reach only 6.13% after 40 days.

Bacterial inoculum samples were taken and analyzed to determine the types of bacteria and to assess the potential inhibitory effect of $Fe_3O_4$ (Fig. 8). As shown in Table 7 and Fig. 9,

Table 8 Comparison in biogas production[a]

| Substrate | mL $CH_4$/g VSs* | mL $CH_4$/g COD** | Time (days) | Temperature (°C) |
|---|---|---|---|---|
| Guinea pig manure (blank- pol-$Fe_3O_4$) - modeling | 1386 | 32 | 40 | 37.5 ± 0.5 |
| Guinea pig manure (blank- cop-$Fe_3O_4$) - modeling | 1583 | 274 | 40 | 37.5 ± 0.5 |
| Guinea pig manure (pol-$Fe_3O_4$) - modeling | 2021 | 47 | 40 | 37.5 ± 0.5 |
| Guinea pig manure (cop-$Fe_3O_4$) - modeling | 1680 | 291 | 40 | 37.5 ± 0.5 |
| Guinea pig manure (blank- pol-$Fe_3O_4$) | 869 | 20 | 7 | 37.5 ± 0.5 |
| Guinea pig manure (blank- cop-$Fe_3O_4$) | 1166 | 202 | 14 | 37.5 ± 0.5 |
| Guinea pig manure (pol-$Fe_3O_4$) | 1402 | 33 | 7 | 37.5 ± 0.5 |
| Guinea pig manure (cop-$Fe_3O_4$) | 1277 | 221 | 14 | 37.5 ± 0.5 |
| Cow manure[48] | 168 | | 90 to 180 | 37 ± 1 |
| Mink manure[48] | 512 | | 90 to 180 | 37 ± 1 |
| Cattle excrement[49] | — | 300 | 7.3 | Mesophilic (30 to 38) |
| Domestic solid waste[50] | — | 882 (mL biogas) | Continuous | 35 ± 1 |
| Municipal solid waste[51] | 360 | | Continuous | 35 ± 2 |
| Rice straw[52] | 178 | 356 | 40 | 37 |
| Corn straw[53] | 217 | | 35 | 37 ± 1 |
| Wheat straw in co-digestion with fungi[54] | 269 | 269 | 62 | 37 |
| Fallen leaves[55] | 82 | 21 | 30 | 37 |
| Garden waste[56] | 45 | 11 | 40 | 37 ± 1 |
| Pig manure[57] | 127 | 212 | 30 | 32 |
| Pig manure[58] | 247 | 412 | 60 | 32 |

[a] *VSs: volatile solids, ** COD: chemical oxygen demand.

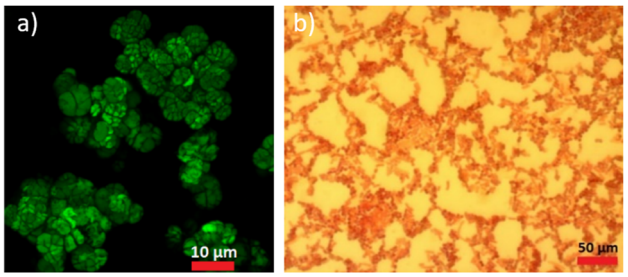


Fig. 9 Benchmark of *Methanosarcina* bacteria in culture. (a) Bacteria *Methanosarcina barkeri* reported in the literature.[58] (b) *Methanosarcina* colonies found in the experiment.

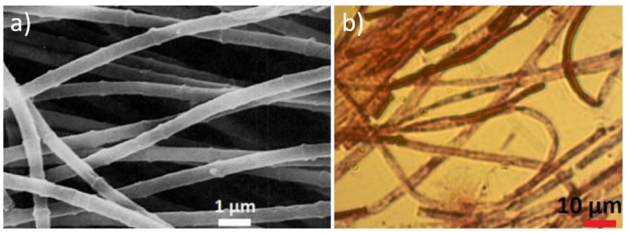


Fig. 10 Benchmark of *Methanothrix* bacteria in culture. (a) *Methanothrix* sp. As reported in the literature.[58] (b) *Methanothrix* colonies found in the experiment.

the bacteria exhibited no inhibition in the presence of $Fe_3O_4$. These findings are corroborated by other studies, which confirm that $Fe_3O_4$ is not inhibitory but rather highly biocompatible with methanogenic bacteria.[43]

Two main bacterial strains were identified, corresponding to methanogenic bacteria. *Methanosarcina* species were found, which are characteristic of ruminants. They primarily metabolize $CH_3COO^-$, $C_2H_5OH$ and $NH_2CH_3$, converting these into $CH_4$. They thrived at temperatures between 30 °C and 45 °C and at a pH between 5.0 and 7.4. They were observed to be immobile and grouped in cell aggregates, as shown in Fig. 9.[58]

The other strain identified was *Methanothrix* (Fig. 10). These are Gram-negative bacteria, filamentous in shape and measuring several micrometres in length. They are characterized by their ability to degrade $CH_3COO^-$ into $CH_4$ and $CO_2$ and are incapable of degrading other substrates.[44,59]

## Conclusions

To conclude, the trials clearly demonstrate the effect of adding $Fe_3O_4$ in 100 ppm on $CH_4$ production. Smaller $Fe_3O_4$ particles (34 nm) showed an increase of up to 64.5% in total $CH_4$ production compared with the Group 2 control reactor. Regarding cop-$Fe_3O_4$ (average size 0.4 μm), a slight increase of up to 9.61% was observed in the total $CH_4$ production compared with the Group 1 control reactor. Notably, $Fe_3O_4$ also significantly affects lag time by reducing it. Although with cop-$Fe_3O_4$, the effect is negligible (a reduction of 0.13 days or 3 hours). When comparing trials with a smaller initial organic load over 7 days (Group 1 = 5.57 g COD initial), a higher biodegradability percentage was achieved compared with Group 2, which had a greater initial load (34.47 g). This highlights the importance of avoiding biodigester overloading with excessive substrate to ensure a more efficient COD removal process. Furthermore, nanoscale magnetite enhances biogas production regardless of the organic load, although its effects are best seen at higher loads (pol-$Fe_3O_4$). Finally, in the three regions of Peru (coast, Andes and Amazonia) household biogas production is feasible owing to abundant guinea pig farms, and the addition of $Fe_3O_4$ to guinea pig manure could help address energy needs in these remote areas.

## Data availability

https://www.drive.google.com/drive/folders/1k9sdaxQYGRHHUZfbE6r2ipNFfTMsWlto?usp=drive_link.

## Author contributions

Rosa Flores Vargas: formal analysis, investigation, methodology, validation, writing-original draft, and visualization; William Eduardo Gómez Hernández: investigation and methodology; Karenina Ela Macazana López: investigation, methodology, and manuscript correction; Clemente Alfredo Luyo Caycho: resources and investigation; Yelstin Adrian Muñoz Baca: resources and investigation; Harry Anderson Rivera Tito: investigation and manuscript correction and María Esther Quintana Cáceda: conceptualization, formal analysis, funding, and writing–review & editing.

## Conflicts of interest

The authors declare that they have no competing interests.

## Acknowledgements

This research has been financed by PROCIENCIA, CONCYTEC and SENCICO through project 123-2018-FONDECYT. We extend our gratitude to the professors and researchers of the Science Faculty—Ronny Huamani, Bryan Córdova, Iván Luyo, Pilar García and Henry Huanca—for their contributions as well as Carmen Felipe-Morales and Jaime Villa for their guidance and expertise in biodigester development. Finally, we thank the Thin Films Lab, URPUNANO group and CEMAT for the facilities provided.

## References

1 F. N. Rohstoffe e. V. (FNR), *Guía sobre el Biogás: Desde la producción hasta el uso*, 5a ed., Gülzow, 2010.
2 P. G. K. y I. Angelidaki, Biogas and its opportunities—A review, *Front. Environ. Sci. Eng.*, 2018, **12**, 14.
3 FAO, *Manual de biogás*, Ministerio de Energía del Gobierno de Chile, Programa de las Naciones Unidas para el Desarrollo, Organización de las Naciones Unidas para la Alimentación y la Agricultura, Global Environment Facility, 2011.

4 G. Casanovas, F. Della, F. Reymundo and R. Serafini, *Guía teórico-práctica sobre el biogás y los biodigestores*, Food and Agriculture Organization of the United Nations (FAO), Rome, 2019, Available from: https://openknowledge.fao.org/handle/20.500.14283/CA7005ES.
5 V. García, *Manual de Biogás: Conceptos básicos, beneficios de su producción y la aplicación de sus sub-productos*, 9ª ed., Dirección de Sustentabilidad, Medio Ambiente y Cambio Climático, Buenos Aires, 2015.
6 M. J. Asgari and K. S. y F. Mortazaeinezhad, Landfill Biogas Production Process, *2011 International Conference on Food Engineering and Biotechnology, IPCBEE*, IACSIT Press, Singapore, 2011, 9.
7 M. Calero, V. Godoy, C. García Heras, E. Lozano and S. A. y M. A. Martín-Lara, Current state of biogas and biomethane production and its implications for Spain, *Sustainable Energy Fuels*, 2023, **7**, 3584–3602.
8 Propuesta Ciudadana, *Balance de las políticas vinculadas a la transición energética en el Perú 2019-2022*, Propuesta Ciudadana, Lima, 2023 [cited 2025 May 1], Available from: https://propuestaciudadana.org.pe/wp-content/uploads/2023/06/Balance-de-las-pol%C3%ADticas-vinculadas-a-la-transici%C3%B3n-energ%C3%A9tica-en-el-Per%C3%BA-2019-2022.pdf.
9 E. Salazar Vega, «*El lento avance del Perú para renovar su matriz energética por recursos limpios,*» 2021. [En línea]. Available: https://www.ojo-publico.com/3106/el-lento-avance-del-peru-para-renovar-su-matriz-energetica.
10 MINEM, *Balance Nacional de Energía*, 2022.
11 El Peruano, «*Energías renovables: cambio necesario con visión de futuro para asegurar sostenibilidad,*» 2022. [En línea]. Available: https://www.elperuano.pe/noticia/198353.
12 R. Orrego Moya, Estado del Arte y Novedades de la Bioenergía en el Perú, vol. *Organización de las Naciones Unidas para la Alimentación y la Agricultura*, 2011.
13 E. Monteros Curiel, L. C. Durand Moreno y and C. Martin del Campo Moreno, *Nanopartículas de hierro magnetizado en la producción de biogás de excretas de ganado porcino*, Tecnogestión, 2019, vol. 16(1), pp. 38–39, [cited 2025 May 1], Available from: https://revistas.udistrital.edu.co/index.php/tecges/article/download/14603/14643/72056.
14 Y. Hu, F. Wang and G. Lv y Y. Chi, Enhancing the Biogas Production of Sludge Anaerobic Digestion by a Combination of Zero-Valent Iron Foil and Persulfate, *Energy Fuels*, 2019, **33**, 7436–7442.
15 E. Casals, R. Barrena, A. García, E. González, L. Delgado, M. Busquets-Fité, X. Font, J. Arbiol, P. Glatzel, K. Kvashnina and A. S. y. V. Puntes, Programmed Iron Oxide Nanoparticles Disintegration in Anaerobic Digesters Boosts Biogas Production, *Small*, 2014, **10**, 2801–2808.
16 M. E. Huamán Córdova, H. L. de Castro e Silva, R. M. Barros, E. E. Silva Lora, I. F. Silva dos Santos, J. V. Rocha de Freitas, A. H. Moreira Santos, J. R. Pedreira and y B. K. Flauzino, Analysis of viable biogas production from anaerobic digestion of swine manure with the magnetite powder addition, *Environ. Technol. Innovation*, 2022, **25**, 102207.
17 J. E. Martí Herrero, *Biodigestores Tubulares: Guía de diseño y Manual de instalación*, RedBioLAC, Ecuador, 2019 [cited 2025 May 1], Available from: http://repositorio.ikiam.edu.ec/jspui/handle/RD_IKIAM/351.
18 T. Montes, Asistencia técnica dirigida en crianza tecnificada de cuyes., *de 2.Trabajo presentado en Cajabamba por parte de la Universidad Nacional Agraria La Molina*, Oficina Académica de Extensión y Proyección Socia, Cajamarca, 2015, vol. 1.
19 L. Villargaray and V. Alvares, Cantidad y calidad del estiércol producido por el cuy (cavia porcellus) alimentados con rye Grass y alfalfa, 1994.
20 C. Felipe-Morales and U. Moreno, Biogas production with guinea pig manure, *LEISA: ILEIA newsletter for low-external-input and sustainable agriculture*, LEISA, 2005, vol. 21(1), p. 16, Available from: https://library.wur.nl/WebQuery/groenekennis/1756019.
21 Ministerio de Desarrollo Agrario y Riego, Cadena productiva de Cuy, vol. Dirección de estudios económicos. *Dirección general de políticas agrarias*., 2023.
22 C. A. de Lemos Chernicharo, *Anaerobic Reactors, Biological Wastewater Treatment Series*, IWA Publishing, London/New York, 2007, vol. 4.
23 C. A. de Lemos and C. y T. Bressani-Ribeiro ed., *Anaerobic Reactors for Sewage Treatment: Design, Construction and Operation*, IWA Publishing, 2019.
24 E. D. Cendales Ladino, *Producción de biogás mediante la codigestión anaeróbica de la mezcla de residuos cítricos y estiércol bovino para su utilización como fuente de energía renovable*, Tesis Doctoral, 2011.
25 S. Laurent, D. Forge, M. Port, A. Roch, C. Robic, L. Vander Elst and R. N. Muller, Magnetic Iron Oxide Nanoparticles: Synthesis, Stabilization, Vectorization, Physicochemical Characterizations, and Biological Applications, *Chem. Rev.*, 2008, **108**, 2064–2110.
26 T. Ahn, J. H. Kim, H.-M. Yang, J. W. Lee and y J.-D. Kim, Formation Pathways of Magnetite Nanoparticles by Coprecipitation Method, *J. Phys. Chem. C*, 2012, **116**(10), 6069–6076.
27 K. P. y A. Sirivat, Synthesis and characterization of magnetite nanoparticles *via* the chemical co-precipitation method, *Mater. Sci. Eng. B*, 2012, **177**, 421–427.
28 A.-G. Niculescu and C. C. y A. M. Grumezescu, Magnetite nanoparticles: Synthesis methods-A comparative review, *Methods*, 2022, **199**, 16–27.
29 M. Puca Pacheco, M. Guerrero Aquino, E. Tacuri Calanchi and R. G. Lopez Campos, Síntesis y caracterización de nanopartículas superparamagnéticas obtenidas por precipitación en microemulsión inversa para aplicaciones biomédicas, *Rev. Soc. Quim. Peru*, 2013, **79**, 99–106.
30 M. Naito, T. Yokohama and K. H. y K. Nogi, *Nanoparticle Technology Handbook*, Elsevier, 2018.
31 W. Cai and J. Wan, Facile synthesis of superparamagnetic magnetite nanoparticles in liquid polyols, *J. Colloid Interface Sci.*, 2007, **305**, 366–370.
32 A. Kotoulas, C. Dendrinou-Samara and M. A. y O. Kalogirou, The Effect of Polyol Composition on the Structural and Magnetic Properties of Magnetite Nanoparticles for

Magnetic Particle Hyperthermia, *Materials*, 2019, **12**(17), 2663.

33 J. R. Vega Chacón, *Influencia de los parámetros experimentales de síntesis en la formación de nanopartículas de magnetita preparadas por método poliol*, Tesis de titulación, 2020.

34 V. E. Córdoba, D. G. Ibarlucía and E. M. Santalla, Desarrollo y validación de un mecanismo para remover $CO_2$ y cuantificar la producción de $CH_4$ en sistemas de digestión anaeróbica, *RedBioLAC*, 2022, **07**, 2393–7394.

35 J. Vega, G. Picasso, L. Avilés Félix and A. López, Influencia de las variables experimentales de preparación en la obtención de nanopartículas de magnetita por el método de descomposición térmica, *Rev. Soc. Quim. Peru*, 2013, **79**, 331–347.

36 U. Schwertmann and y R. M. Cornell, *Iron Oxides in the Laboratory*, vol. 173, Weinheim: Wiley-VcH, 1991.

37 A. Ghosh and V. S. y R. Sundara, Comprehensive structural and magnetic properties of iron oxide nanoparticles synthesized through chemical routes, *J. Alloys Compd.*, 2020, **818**, 152931.

38 Nature Nanotechnology, "Broadening of diffraction peaks and its implications," *Nat. Nanotechnol.*, 2011. [Online]. Available: **https://www.nature.com/articles/nnano.2011.145**.

39 B. Kalska-Szostko, D. Satula and W. Olszewski, Mössbauer spectroscopy studies of the magnetic properties of ferrite nanoparticles, *Curr. Appl. Phys.*, 2015, **15**, 226–231.

40 G. Peña-Rodríguez, P. A. Rivera-Suárez, C. H. González-Gómez, C. A. Parra-Vargas, A. O. Garzón-Posada, D. A. Landínez-Téllez and J. Roa-Rojas, Efecto de la concentración de magnetita en la estructura, propiedades eléctricas y magnéticas de un material compuesto a base de resina de poliéster, *Tecno Lógicas*, 2018, **21**(41), 13–27.

41 B. J. Berne and R. Pecora, *Dynamic Ligh Scattering with Applications to Chemistry, Biology, and Physics*, Wiley - Interscience, New York, 1976.

42 E. Al-Essa, R. Bello-Mendoza and D. G. Wareham, The effect of magnetite particle size on methane production by fresh and degassed anaerobic sludge, *Int. J. Environ. Ecol. Eng.*, 2020, **14**(2), 63–66.

43 Y. Xu, Y. Lu, X. Dai, M. Liu, L. Dai and B. Dong, Spatial Configuration of Extracellular Organic Substances Responsible for the Biogas Conversion of Sewage Sludge, *ACS Sustainable Chem. Eng.*, 2018, **6**, 8308–8316.

44 C. Cruz Viggi, S. Rossetti, S. Fazi, P. Paiano, M. Majone and F. Aulenta, Magnetite particles triggering a faster and more robust syntrophic pathway of methanogenic propionate degradation, *Environ. Sci. Technol.*, 2014, **48**(13), 7536–7543.

45 G. Baek, J. Kim and C. Lee, A review of the effects of iron compounds on methanogenesis in anaerobic environments, *Renewable Sustainable Energy Rev.*, 2019, **113**, 109282.

46 Z. Wang, T. Wang, B. Si, J. Watson and Y. Zhang, Accelerating anaerobic digestion for methane production: Potential role of direct interspecies electron transfer, *Renewable Sustainable Energy Rev.*, 2021, **145**, 111069.

47 V. Rumyantceva, V. Rumyantceva, E. Koshel and V. Vinogradov, Biocide-conjugated magnetite nanoparticles as an advanced platform for biofilm treatment, *Ther. Deliv.*, 2019, **10**(4), 241–250.

48 V. Dubrovskis, I. Plume and I. Straume, Investigation of biogas production from mink and cow manure, *Presented at Latvia University of Agriculture*, Jelgava, Latvia, 2009.

49 L. Castrillón, I. Vázquez and E. M. y H. Sastre, Anaerobic thermophilic treatment of cattle manure in UASB reactors, *Waste Manage. Res.*, 2002, **20**, 350–356.

50 J. Lebrato, J. L. Pérez-Rodríguez and y C. Maqueda, Domestic solid waste and sewage improvement by anaerobic digestion: a stirred digester, *Resour. Conserv. Recycl.*, 1995, **13**, 83–88.

51 F. Cecchi and P. G. T. y P. Cescon, Anaerobic digestion of organic fraction of municipal solid wastes-digester performance, *Sci. Total Environ.*, 1986, **56**, 183–197.

52 Y. Gu, X. Chen, Z. Liu and X. Z. y Y. Zhang, Effect of inoculum sources on the anaerobic digestion of rice straw, *Bioresour. Technol.*, 2014, **158**, 149–155.

53 Z. Song, G. Yang, X. Liu, Z. Yan and Y. Y. y Y. Liao, Comparison of seven chemical pretreatments of corn straw for improving methane yield by anaerobic digestion, *PLoS One*, 2014, **9**, e93801.

54 J. Zhu and C. W. y Y. Li, Enhanced solid-state anaerobic digestion of corn stover by alkaline pretreatment, *Bioresour. Technol.*, 2010, **101**, 7523–7528.

55 Y. Lin and X. Ge y Y. Li, Solid-state anaerobic co-digestion of spent mushroom substrate with yard trimmings and wheat straw for biogas production, *Bioresour. Technol.*, 2014, **169**, 468–474.

56 J. Zhao and Y. Z. y Y. Li, Fungal pretreatment of yard trimmings for enhancement of methane yield from solid-state anaerobic digestion, *Bioresour. Technol.*, 2014, **156**, 176–181.

57 C. González-Fernández, C. León-Cofreces y and P. A. García-Encina, Different pretreatments for increasing the anaerobic biodegradability in swine manure, *Bioresour. Technol.*, 2008, **99**, 8710–8714.

58 S. C. Lambie, W. J. Kelly, S. C. Leahy, D. Li, K. Reilly, T. A. McAllister, E. R. Valle, G. T. Attwood and E. Altermann, The complete genome sequence of the rumen methanogen Methanosarcina barkeri CM1, *Stand. Genomic Sci.*, 2015, **10**, 57.

59 J. P. Touzel, G. Prensier, J. L. Roustan, I. Thomas, H. C. Dubourguier and G. Albagna, Description of a New Strain of Methanothrix soehngenii and Rejection of Methanothrix concilii as a Synonym of Methanothrix soehngenii, *Int. J. Syst. Evol. Microbiol.*, 1988, **38**, 30–36.